Near-Field Scanning Optical Microscopy of Temperature- and Thickness-Dependent Morphology and Fluorescence in Alq_3 Films

Grace M. Credo, Darby L. Winn, and Steven K. Buratto*

Department of Chemistry and Biochemistry, University of California at Santa Barbara, Santa Barbara, California 93106-9510

Received August 21, 2000

We use near-field scanning optical microscopy (NSOM) to probe the local optical and morphological properties in annealed, vacuum-deposited Alq_3 films (10−480-nm thick) with 10−100-nm resolution. We use concurrent shear force microscopy (an analogue to atomic force microscopy, AFM) to correlate the morphology of different regions to intensity variations in our fluorescence images as well as variations in the localized fluorescence spectra. We have observed nanoscale effects of annealing temperature on film morphology and fluorescence emission. Our studies show that Alq_3 films annealed below the glass transition temperature of Alq_3 ($T < T_g = 172$ °C) were very similar to unannealed films, except in very thin films (<50 nm). Films annealed above T_g ($T = 200$ °C) for the same amount of time exhibit increased surface morphology and decreased fluorescence. In sufficiently thick films (≈500 nm) annealed at 200 °C, we observe the formation of microcrystalline domains.

Introduction

Because the use of a thin film of vacuum-deposited tris-8-hydroxyquinoline aluminum (Alq_3) as the emissive layer in a practical electroluminescent device constructed from layered organic materials was first demonstrated in 1987,[1] the experimental and theoretical properties of Alq_3 have been widely studied.[2−8] When compared to inorganic III−V semiconductors, molecular organic semiconductors, such as Alq_3, offer the possibility of flexible commercial displays, more facile wide-area film deposition, cheaper purification costs, and more versatile color specificity. For over a decade, a variety of approaches have been used to better understand the optical and charge transport properties of Alq_3 films. Recently, this work resulted in Alq_3-based small-area commercial displays for car stereos from Pioneer Electronics (http://www.pioneerelectronics.com). However, despite the numerous spectroscopy techniques applied to Alq_3 films, the dependence of optical properties on Alq_3 film morphology, particularly on a submicron level, remains poorly understood.[9,6]

Previous studies rely on far-field spectroscopy techniques that average over many morphological domains[10−12] or on topographical images taken without the benefits of concurrent optical probing.[13] Previous temperature studies of Alq_3 thin films have combined far-field spectroscopy with bulk techniques such as differential scanning calorimetry (DSC) and X-ray diffractometry (XRD).[14] While these techniques provide important information about phase transitions and sample crystallinity, respectively, they are not able to provide the nanoscale morphology and fluorescence variation information that is possible with near-field scanning optical microscopy (NSOM). In particular, Alq_3 samples used for DSC and XRD analysis are ≈2-mm thick,[14] much thicker than those used in devices. As we will describe, in films much less than 2-mm thick, we have observed dramatic changes in morphology and fluorescence emission efficiency after thermal annealing and these changes vary with initial film thickness.

In this work, we apply near-field scanning optical microscopy (NSOM) to *directly* probe the nanoscale (10−100 nm) optical properties of annealed Alq_3 thin films between 10- and 480-nm thick. Our results complement previous NSOM studies of Alq_3/TPD-based device deg-

(1) Tang, C. W.; Van Slyke, S. A. *Appl. Phys. Lett.* **1987**, *51*, 913−915.
(2) Sheats, J. R.; Antoniadis, H.; Hueschen, M.; Leonard, W.; Miller, J.; Moon, R.; Roitman, D.; Stocking, A. *Science* **1996**, *273*, 884−888.
(3) Aziz, H.; Popovic, Z. D.; Hu, N.-X.; Hor, A.-M.; Xu, G. *Science* **1999**, *283*, 1900−1902.
(4) Curioni, A.; Boero, M.; Andreoni, W. *Chem. Phys. Lett.* **1998**, *294*, 263−271.
(5) Brinkmann, M.; Gadret, G.; Muccini, M.; Taliani, C. *J. Am. Chem. Soc.* **2000**, *122*, 5147−5157.
(6) Cheng, L. F.; Liao, L. S.; Lai, W. Y.; Sun, X. H.; Wong, N. B.; Lee, C. S.; Lee, S. T. *Chem. Phys. Lett.* **2000**, *319*, 418−422.
(7) Gross, E. M.; Anderson, J. D.; Slaterbeck, A. F.; Thayumanavan, S.; Barlow, S.; Zhang, Y.; Marder, S. R.; Hall, H. K.; Nabor, M. F.; Wang, J.-F.; Mash, E. A.; Armstrong, N. R.; Wightman, R. M. *J. Am. Chem. Soc.* **2000**, *122*, 4972−4979.
(8) Kushto, G. P.; Iizumi, Y.; Kido, J.; Kafafi, Z. H. *J. Phys. Chem. A* **2000**, *104*, 3670−3680.
(9) Jabbour, G. E.; Y. Kawabe, S. E. S.; Wang, J. F.; Morrell, M. M. Kippelen, B.; Peyghambarian, N. *Appl. Phys. Lett.* **1997**, *71*, 1762−1764.
(10) Fujihira, M.; Do, L.-M.; Koike, A.; Han, E.-M. *Appl. Phys. Lett.* **1996**, *68*, 1787−1789.
(11) Papadimitrakopoulos, F.; Zhang, X. M.; Thomsen, D. L.; Higginson, K. A. *Chem. Mater.* **1996**, *8*, 1363−1365.
(12) Walser, A. D.; Sokolik, I.; Priestley, R.; Dorsinville, R. *Synth. Met.* **1997**, *84*, 877−878.
(13) Yase, K.; Sumimoto, S.-S.; Matsuda, H.; Kato, M. *Mol. Cryst. Liq. Cryst.* **1995**, *267*, 151−156.
(14) Higginson, K. A.; Zhang, X. M.; Papadimitrakopoulos, F. *Chem. Mater.* **1998**, *10*, 1017−1020.

10.1021/cm000672o CCC: $20.00
Published on Web 03/06/2001

radation reporting micron-size features,[10] atomic force microscopy (AFM) studies of Alq_3 and TPD layers on indium−tin oxide (ITO),[15,6] transmission electronic microscopy (TEM) of Alq_3 on various substrates,[13] and NSOM studies on as-deposited (unannealed) Alq_3 thin films from our group that are reported elsewhere.[16]

Experimental Section

Materials Used and Film Deposition. Glass coverslips (0.17-μm thick, Fisher) were used as sample substrates. The slides were rinsed in acetone and flamed before use. Alq_3 powdered solid was used as-delivered (Aldrich). The solids were placed in a baffled tungsten evaporating boat (R. D. Mathis) and sublimed at low pressures ($\approx 10^{-6}$ Torr). Film thicknesses were monitored by a quartz crystal thickness monitor. Samples were annealed by placing them in a sample holder in an oven for 60 min, after the oven had been equilibrated for 30 min at the desired temperature. Samples were stored and scanned in ambient conditions. Sample thicknesses before and after annealing were measured by standard profilometry (Sloan Dektak II).

Near-Field Scanning Optical Microscopy. In NSOM, a subwavelength (10−200 nm) aperture was placed in close proximity to the surface of interest (near-field region ≈ 10 nm) and the interaction between laser light passing through the aperture and the sample was limited to the aperture diameter.[17] If the aperture is maintained in the near-field and scanned over a sample surface, an image can be reconstructed point by point with spatial resolution limited by the aperture diameter rather than by the wavelength of light (the diffraction limit, $\lambda/2$). The combination of the proximity of the tip to the sample and small tip aperture in NSOM made it possible to achieve ultrahigh spatial resolution.

In our NSOM apparatus, depicted in Figure 1, a tapered fiber optic tip with laser light coupled to it was fixed while the sample, mounted film-side down on a piezo tube (Stavely Sensors), was raster-scanned above it. The tip was used to excite the sample and the emission (fluorescence) that results in the sample was detected in the far-field using a 125× microscope objective (0.80 NA, Leitz). Using a beam splitter in the path of the transmitted signal, we were able to collect spatially resolved fluorescence spectra simultaneously with integrated fluorescence imaging. Our tip apertures were typically 100 nm in diameter. The tip−sample distance, regulated by the standard optical shear force feedback mechanism, was ≈10 nm.

Shear Force Microscopy. We imaged the topography of the sample simultaneously with NSOM using shear force microscopy, an analogue to attractive mode atomic force microscopy (AFM). In shear force microscopy, the tapered optical fiber NSOM tip (diameter ≈200 nm) was used to scan the surface of the sample.[18] This tip was attached to a small piezoelectric tube and dithered on resonance. The tip−sample distance was determined by monitoring the dither amplitude as the sample approached the tip. The dither amplitude was measured by scattered laser light synchronously with the dither frequency. This provided the input for the feedback loop of our scanning electronics, shown in Figure 1, which was set to maintain a constant height above the sample surface (≈10 nm).

Laser Scanning Confocal Microscopy. Laser scanning confocal microscopy (LSCM) was also used to obtain larger areas scans of the annealed Alq_3 films with spatial resolutions of ≈400 nm. Our laser scanning confocal microscope has been described in detail.[19] For LSCM, the same apparatus depicted in Figure 1 was used with the NSOM tip removed. For excitation the 457.9-nm line of an Ar^+ laser (Spectra-Physics) was directed into the microscope and focused into a small spot using the objective used for NSOM. The resulting fluorescence was detected the same way as fluorescence NSOM, with the APD detector placed confocal with the excitation spot.

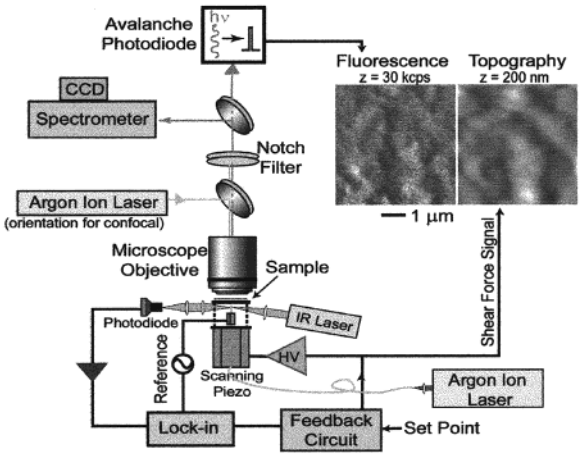

Figure 1. Near-field scanning optical microscopy (NSOM) schematic. The sample is placed on a piezoelectric tube between a high numerical aperture objective and a fiber optic tip (transmission mode NSOM). The photodiode detects (left of the tip in the schematic) IR laser light scattered by the dithered tip. This signal is used for optical shear force detection and is used in a feedback circuit to maintain the tip in the near-field (≈10 nm) of the sample. In addition, this signal is used to map topography images of the sample surface. Transmitted fluorescence is collected in the far-field with the microscope objective. With a beam splitter in the path of the collected fluorescence signal, emission intensity images and emission spectra can be acquired simultaneously.

Absorption and Emission Spectroscopy. Bulk absorption spectra of Alq_3 films were recorded on a diode array absorption spectrophotometer (Hewlett-Packard, 8452A). Near-field scanning optical spectra were obtained using the optical collection setup used for NSOM imaging.

Results and Discussion

Annealing Effects on the Absorption of Alq_3 Thin Films. Alq_3 films of 10, 20, 50, 100, and 480 nm were vacuum-deposited on glass and absorption spectra were taken before annealing, after 60 min at 100°C ($T < T_g$), and after 60 min at 200 °C ($T > T_g$). Examples of absorption spectra of two different films (10-nm thick in Figure 2a and 480-nm thick in Figure 2b) are presented in Figure 2. The unannealed Alq_3 films exhibit characteristic Alq_3 absorption peaks at about 385 and 260 nm. The two prominent bands in the Alq_3 absorption spectrum are attributed to the ^1L_a (385 nm) and ^1B_b (260 nm) electronic transition bands.[20] Previous studies on Alq_3 and other quinoline chelates in solution have determined that Alq_3 absorption and fluorescence are ligand-localized.[21−24] The absorption spectra for

(15) Han, E.-M.; Do, L.-M.; Yamamoto, N.; Fujihira, M. *Mol. Cryst. Liq. Cryst.* **1995**, *267*, 411−416.
(16) Credo, G. M.; Lowman, G. M.; DeAro, J. A.; Carson, P. J.; Winn, D. L.; Buratto, S. K. *J. Chem. Phys.* **2000**, *112*, 7864−7872.
(17) Betzig, E.; Trautman, J. K.; Harris, T. D.; Weiner, J. S.; Kostelak, R. L. *Science* **1991**, *251*, 1468−1470.
(18) Betzig, E.; Finn, P. L.; Weiner, J. S. *Appl. Phys. Lett.* **1992**, *60*, 2484−2486.
(19) Weston, K. D.; Buratto, S. K. *J. Phys. Chem. A* **1998**, *102*, 3635−3638.
(20) Garbuzov, D. Z. B., V.; Burrows, P. E.; Forrest, S. R. *Chem. Phys. Lett.* **1996**, *249*, 433−437.
(21) Ballardini, R.; Varani, G.; Indelli, M. T.; Scandola, F. *Inorg. Chem.* **1986**, *25*, 3858−3865.
(22) Bardez, E.; Devol, I.; Larrey, B.; Valeur, B. *J. Phys. Chem. B* **1997**, *101*, 7786−7793.
(23) Hall, M. D.; Aroca, R. *Can. J. Chem.* **1998**, *76*, 1730−1736.

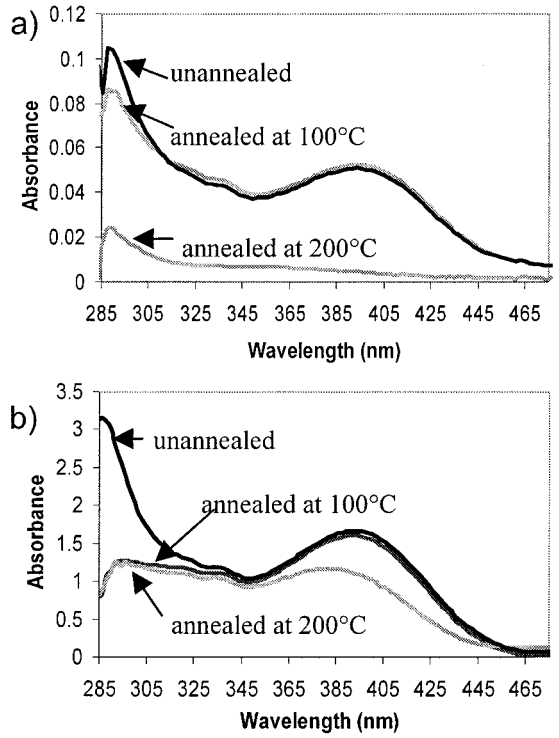

Figure 2. Comparison of bulk absorption spectra of two different vacuum-deposited Alq_3 films with (a) a 10-nm-thick film and (b) a 480-nm-thick film. Each plot shows spectra taken at room temperature before annealing, after annealing for 60 min at 100 °C, and after annealing for 60 min at 200 °C.

metal oxinates such as Alq_3 are nearly identical to those of free 8-hydroxyquinoline.

For the two different film thicknesses, the spectra before annealing and annealing at below the glass transition temperature ($T = 172$ °C)[14] are nearly identical, indicating minimal differences in chemical composition. Both films, annealed at less than the glass transition temperature, exhibit similar absorption spectra to unannealed films. What is remarkable is the disappearance of the absorption peak at 395 nm for the 10-nm-thick film (Figure 2a) but not the 480-nm-thick film (Figure 2b). Although the peak maximum in the absorption spectrum for the 480-nm film shifts toward shorter wavelengths after annealing at greater than T_g, the peak does not disappear as it does in the thinner film. The observed absorption spectrum for the 10-nm-thick film annealed at 200 °C suggests that Alq_3 does not remain on the glass after the anneal. However, we verified that we were not merely subliming the Alq_3 by checking film thicknesses before and after annealing. The two measurements did not vary more than 10%. These results indicated that the thicker Alq_3 films were more thermally stable.

Figure 3a is a plot of the absorbance measured at 395 nm for films between 10- and 480-nm thick. In general, the absorbance increases with thickness; however, for thin films (<50 nm) annealed at 200 °C, absorbance at 395 nm is significantly reduced, indicating a change in the chemical nature of the film after annealing at 200

(24) Burrows, P. E.; Shen, Z.; Bulovic, V.; McCarty, D. M.; Forrest, S. R.; Cronin, J. A.; Thompson, M. E. *J. Appl. Phys.* **1996**, *79*, 7991−8006.

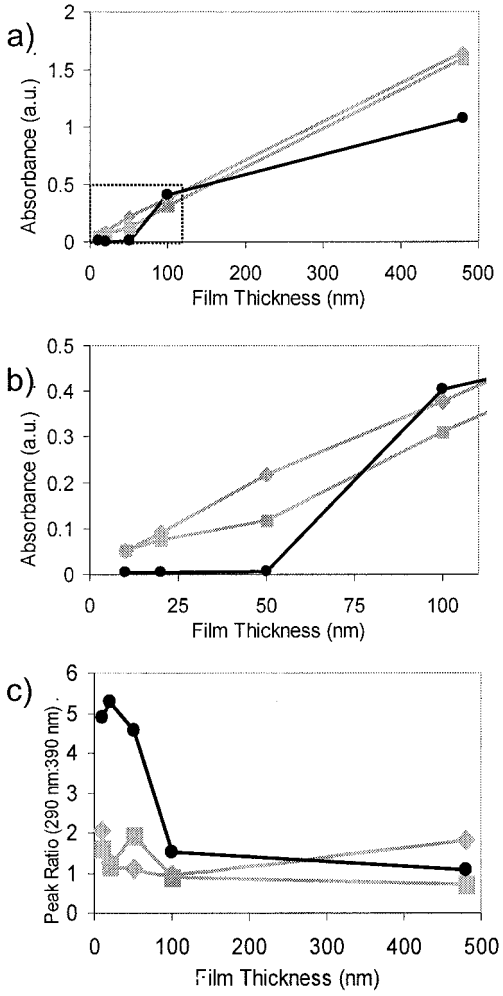

Figure 3. Comparing trends in absorption peak intensity for different film thicknesses. (a) The absorption spectrum intensity at 395 nm for each film thickness was used to compare film absorption before (◆) and after annealing at 100 °C (■) or after annealing at 200 °C (●). A dashed vertical line for annealed and unannealed films between 10- and 480-nm thick denotes the absorbance measured at 395 nm. The graph in (b) is a close-up of the same plot in the region between 10- and 100-nm thick. It highlights the absence of the 395-nm peak for 200 °C annealed films <50-nm thick. (c) A plot of the ratio of the 295-nm absorption peak to the 395-nm absorption peak illustrates another difference between the annealed and unannealed films.

°C. Figure 3b, which illustrates the absence of the 395-nm absorption peak for films much less than 100 nm, is a close-up of Figure 3a. Figure 3c illustrates a related difference between the films annealed above T_g and films annealed below T_g. The ratio of the 295-nm absorption peak to the 395-nm absorption peak is shown in Figure 3c as a function of film thickness. For films <100 nm annealed at 200 °C, this ratio is much larger, ≈5:1 (295-nm peak to 395-nm peak), than that for other annealing conditions and for thicker Alq_3 films, which exhibit peak ratios between 2:1 and 1:1.

The observed difference between the thinner (10 nm) and thicker film (480 nm) absorption was unexpected. Given the observed results, the thicker Alq_3 films exhibit greater thermal stability than the thinner films. Films <50-nm thick, which have been annealed above T_g, undergo more drastic changes in fluorescence efficiency and morphology than thicker films. It is clear from these

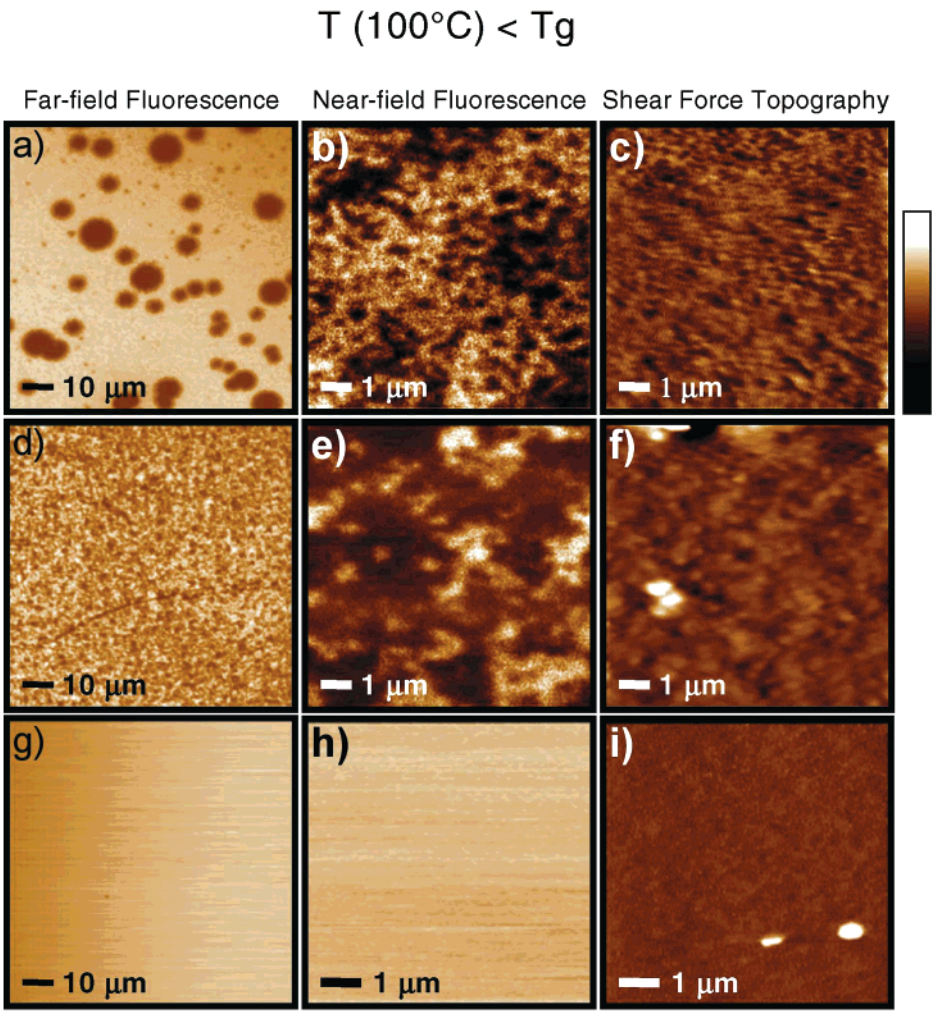

Figure 4. Fluorescence and topography effects after annealing three different Alq_3 films at $T < T_g$ for 60 min. Far-field fluorescence micrographs (left-hand column), concurrently obtained NSOM fluorescence (middle column), and shear force topography (right-hand column) images of three different thicknesses of Alq_3 films. The following thicknesses refer to the film before annealing: (a)−(c) 15 nm, (c)−(e) 50 nm, and (f)−(i) 480 nm. Using the scale bar at the top right, the *z*-scales for each image are as follows: (a) 1000 kcps, (b) 10 kcps, (c) 20 nm, (d) 2000 kcps, (e) 20 kcps, (f) 30 nm, (g) 8000 kcps, (h) 2000 kcps, and (i) 20 nm. The signal levels in the far-field fluorescence images (left-hand column) are not directly comparable, as the laser intensity was varied to enhance the contrast. The NSOM and shear force images, obtained with the same tip, are comparable.

spatially averaged absorption measurements that annealing Alq_3 films influences the optical properties of the material. To understand these effects in more detail, we conducted high-resolution fluorescence and topography studies on these films using NSOM.

Films Annealed at $T < T_g$. As shown in previous studies, unannealed vacuum-deposited Alq_3 thin films exhibit homogeneous fluorescence (rms < 3 kcps) and topography (rms < 1 nm).[25] The far-field UV/vis absorption spectra of films annealed at less than T_g in Figure 2 indicated that these annealed films are very similar to unannealed films. In contrast, far-field fluorescence microscopy, NSOM, and topography images of films annealed at less than T_g has revealed significant unexpected differences in both fluorescence and topography from unannealed films.

Although we have found that in films on the order of hundreds of nanometers thick, annealing at 100 °C for 60 min does not decrease the fluorescence efficiency, Figure 4 shows that this is not the case for thinner films (<100 nm). Figure 4 contains far-field fluorescence, NSOM, and shear force topography images from Alq_3 films of different thicknesses. Note that the lateral scale bars on the far-field fluorescence images (far left) are 10 times those of the NSOM (middle column) and topography (far right) images.

Parts a−c of Figure 4 are microscopy images of a 15-nm-thick film. Figure 4a is characteristic of electroluminescence (EL) and photoluminescence (PL) images taken of degraded LEDs.[26,10] In organic LEDs using Alq_3 as the emissive layer, dark spots visible in both PL and EL micrograph images are known to form after operation and these areas grow larger with continued use.[10] In these studies, the EL and PL dark spots are not necessarily present in the same regions, but this is to be expected as the transport processes that contribute to each mechanism are not the same. The NSOM (Figure 4b) and concurrently obtained shear force (Figure 4c) images reveal that the near-field fluorescence also varies on a submicron scale and the topography exhibits many variations that correlate one to one

(25) Credo, G. M.; Buratto, S. K. *Adv. Mater.* **2000**, *12*, 183−186.

(26) Aziz, H.; Popovic, Z.; Xie, S.; Hor, A. M.; Hu, N. X.; Tripp, C.; Xu, G. *Appl. Phys. Lett.* **1998**, *72*, 756−758.

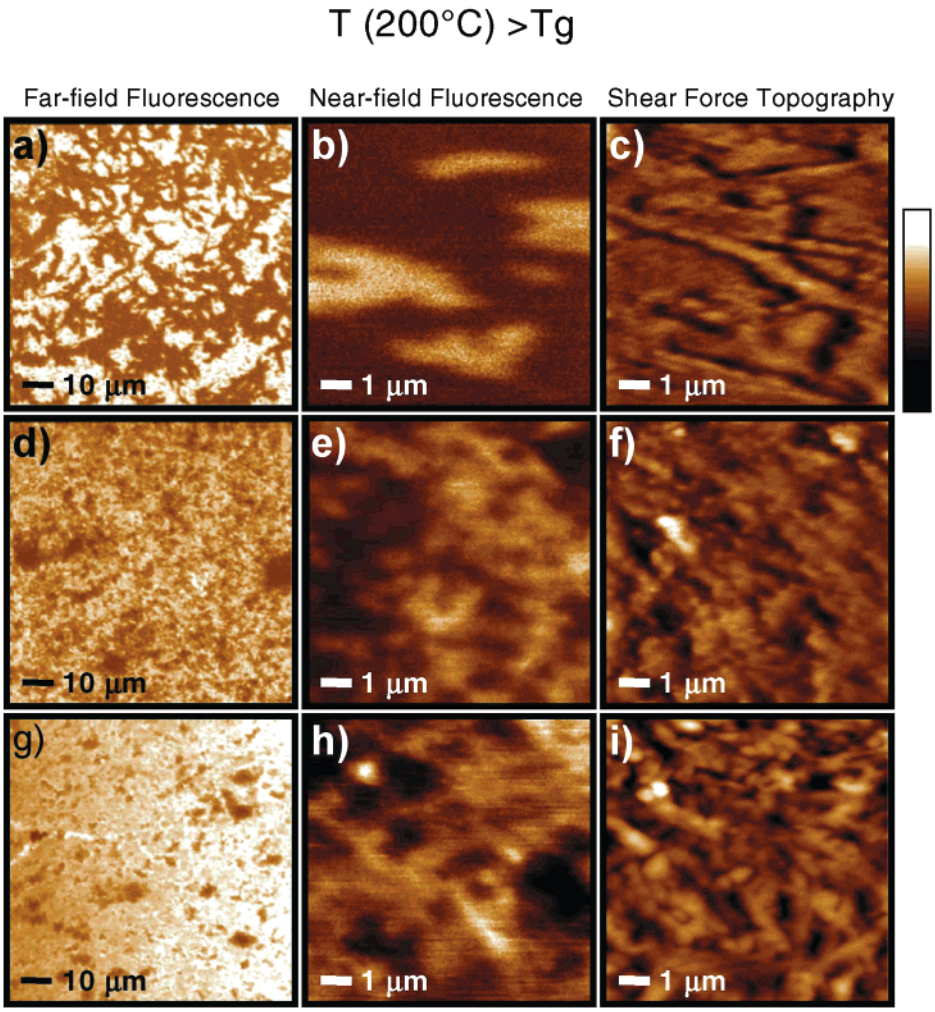

Figure 5. Fluorescence and topography effects after annealing three different Alq_3 films at $T > T_g$ for 60 min. Far-field fluorescence micrographs (left-hand column), concurrently obtained NSOM fluorescence (middle column), and shear force topography (right-hand column) images of three different thicknesses of Alq_3 films. The following thicknesses refer to the film before annealing: (a)−(c) 15 nm, (c)−(e) 50 nm, and (f)−(i) 480 nm. Using the scale bar at the top right, the *z*-scales for each image are as follows: (a) 90 kcps, (b) 25 kcps, (c) 20 nm, (d) 1200 kcps, (e) 120 kcps, (f) 50 nm, (g) 500 kcps, (h) 250 kcps, and (i) 80 nm. The signal levels in the far-field fluorescence images (left-hand column) are not directly comparable, as the laser intensity was varied to enhance the contrast. The NSOM and shear force images, obtained with the same tip, are comparable.

with the darker regions in the NSOM image. However, the variations in the topography image do not completely account for the variations in fluorescence intensity observed in Figure 4b. In addition, we believe that we are scanning a region of the film that would be considered brighter rather than darker in the far-field fluorescence image. Such a region represents a greater percentage of the surface area of this particular film. We do not observe the expected fluorescence contrast if we were scanning the edge of one of the dark spots apparent in Figure 4a.

Parts d−f of Figure 4 are, respectively, far-field fluorescence, NSOM, and shear force microscopy images of a 50-nm-thick film. In Figure 4d, there are darker areas of the far-field fluorescence image of the film, but these are no longer large round dark spots as seen in Figure 4a. In contrast to the 15-nm-thick film, there appears to be phase segregation of a brighter Alq_3 and much less fluorescence (by 50%) Alq_3. As in the case of the 15-nm-thick film, the observed contrast in the NSOM image (Figure 4e) is not correlated one to one with the topography features of Figure 4f.

The final series of images (parts g−i of Figure 4) are the far-field fluorescence, NSOM, and shear force topograhpy images of a 480-nm-thick film. The images clearly reveal that, at a sufficient film thickness, annealing at less than the glass transition temperature does not change the film fluorescence homogeneity when compared to that of an unannealed film. The fluorescence and topography vary <1%.

Films Annealed at $T > T_g$. As explained in the previous section, although the bulk absorption spectra for unannealed films and films annealed at less than T_g were nearly identical, the far-field fluorescence microscopy, NSOM, and topography images of films annealed at less than T_g revealed significant unexpected differences in both fluorescence and topography from unannealed films, below a particular film thickness. For films annealed at greater than T_g, we observed significant differences in both bulk absorption spectra and microscopy images when compared to those of the original, unannealed films for all film thicknesses (10−480 nm) in our study.

The Alq_3 films annealed at 200 °C exhibit larger regions of decreased fluorescence efficiency (darker regions in the LSCM images) for a given thickness when compared to films annealed at 100 °C. At elevated temperatures, above the glass transition temperature, dark spots similar to those seen in Figure 4a may have formed, but thermally aided mass transport at 200 °C has appeared to lead to the formation of crystals or crystalline regions in the far-field fluorescence image in Figure 5a. Analogous XRD results in much thicker films confirm the increase in crystallinity with exposure of the film to temperatures greater than T_g for times as low as 20 min.[14]

The corresponding NSOM and topography images reveal phase segregation similar to that observed in Figure 4e, but the aggregates of the brighter fluorescent material are larger. Note that the darker regions are also fluorescing, but the intensity is 50% less. In contrast to the topography images obtained in Figure 4, where the observed differences in fluorescence intensity were not easily correlated to features in the shear force images, Figure 5c does help to understand the corresponding NSOM image. While there are no measurable topography differences, which correspond to the darker and lighter fluorescence, there are depressions in the topography image that correspond to the boundaries of the brighter regions in the NSOM image. When interpreted in this fashion, the brighter regions correspond to islandlike regions in the topography image, while the darker NSOM regions correspond to elongated features in the topography image. The far-field fluorescence image (Figure 5a) suggested that the brighter fluorescence regions consisted of crystalline aggregates of Alq_3. The brighter fluorescence could have been the result of more Alq_3 in a particular region of the film. The corresponding NSOM and topography images do not support this hypothesis. Except for the depressions in the film visible in the topography image, thickness variations do not account for the observed fluorescence variations in the NSOM image. The shear force image indicates that molecular packing or differences in local chemical composition in certain regions of the film may contribute to greater film fluorescence efficiency in Alq_3.[25]

Parts d−f of Figure 5 are microscopy images of a 50-nm-thick film. Again, we observe variations in the fluorescence in both the far-field fluorescence and NSOM images of the annealed film. The NSOM image provides a closer look at the fluorescence variations in the film as well as the corresponding surface topography. As in Figure 5c, the topography image for this film thickness (Figure 5f) reveals that variations in film thickness are not the cause of the larger fluorescence variations in the NSOM image. In particular, the darker region on the left side of the NSOM image does not correspond to a lower or darker region in the topography image.

Microscopy images of a 480-nm-thick annealed film (Figure 5g−i) illustrate similar trends to those observed in the previous images in Figure 5. Notably, this series is very different from the far-field fluorescence, NSOM, and topography images taken of a 480-nm-thick film annealed at less than T_g (Figure 4g−i). Annealing the Alq_3 films at greater than T_g resulted in fluorescence and topography changes in films from 10- to 480-nm thick. In this particular case, the topography image (Figure 5i) demonstrates the presence of elongated, needlelike features, which are most likely crystals of Alq_3.[13,6] The corresponding NSOM images reveal regions of fluorescence that sometimes correspond to the elongated crystals in the topography image, but not all of the apparent crystals in the Alq_3 image are as fluorescent as others. These images also suggest the importance of local order in the annealed Alq_3 film and the effects of this order on fluorescence efficiency.

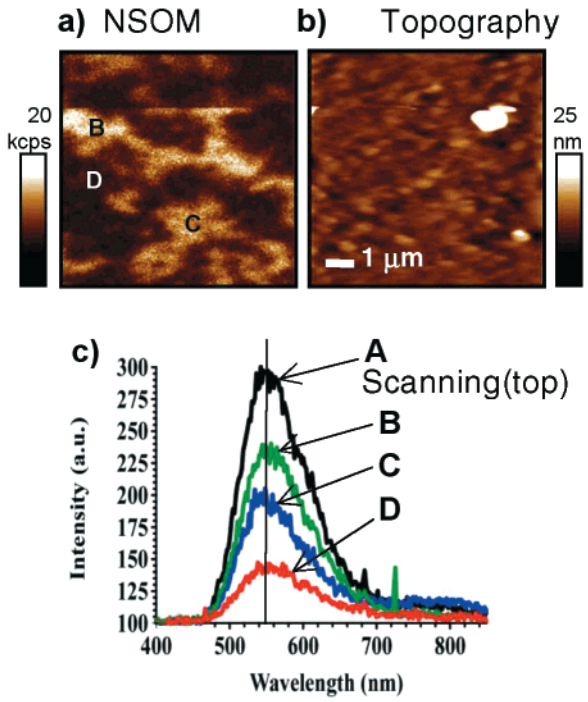

Figure 6. Spatially resolved spectroscopy on a 100-nm-thick Alq_3 film annealed for 60 min at 200 °C. (a) An NSOM fluorescence intensity image with four labeled regions (A, B, C, D). (b) A topography image obtained concurrently. (c) Plot of spectra taken at the points indicated on the NSOM image in (a). Spectrum A was obtained by integrating the collected signal over several lines in the image (scanning) while B, C, and D were obtained at the indicated points (zoomed in, not scanning).

Like previous studies, atomic force microscopy (AFM) studies of Alq_3 films, we have found that film topography does change with annealing temperature, but concurrently obtained fluorescence NSOM images allow us to better understand some of the observed topography features. With sample annealing, the Alq_3 films undergo phase segregation, with distinct regions of bright fluorescence and less intense fluorescence becoming more apparent with increased annealing temperature. What is unexpected is that there is often no obvious topography change denoting one type of region from the other, although local morphology changes may be the cause of the fluorescence efficiency differences. Sometimes boundaries between the two regions can be assigned by comparing the NSOM image with the shear force image, but this is not always the case.

Spatially Resolved Spectroscopy of Annealed Alq_3 Films. Another way to determine the nature of fluorescent regions within an NSOM or far-field fluorescence image is to evaluate concurrently obtained fluorescence spectra from regions of different fluores-

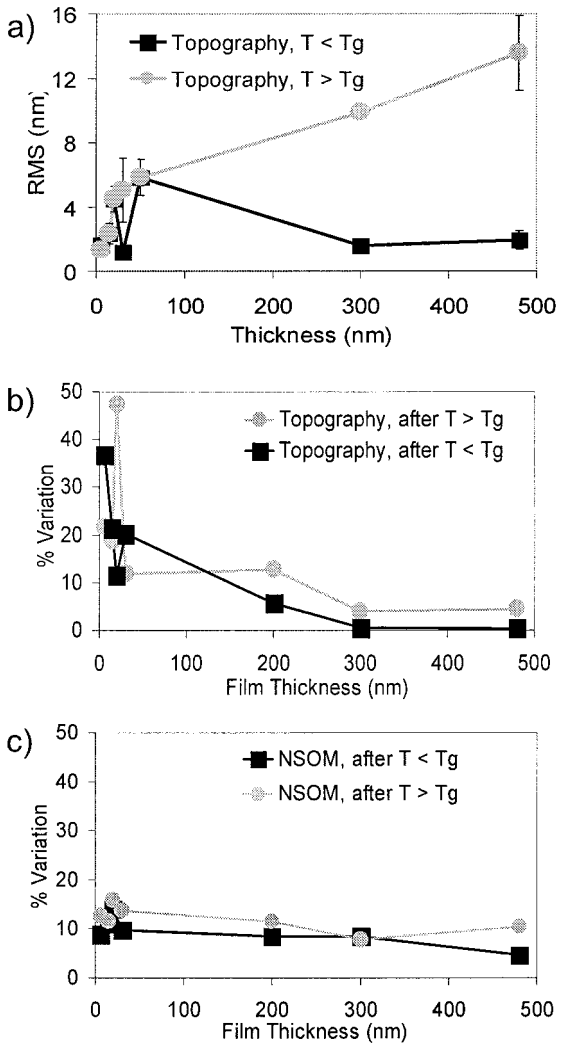

Figure 7. Evaluating variations in fluorescence intensity and surface topography using rms surface roughness. (a) A plot of absolute rms roughness (not adjusted for thickness of film) with increasing film thickness for films after annealing at 100 °C (l) and after annealing at 200 °C (n). For both thin and thicker Alq_3 films annealed at $T < T_g$, the rms surface roughness in nm is relatively constant for films between 10 and 500 nm. For films annealed at $T > T_g$, the rms surface roughness in nm for films between 10- and 500-nm thick increases roughly linearly with film thickness. (b) A graph comparing percent variation in topography for all films annealed below and above T_g. (c) A graph comparing percent variation in fluorescence NSOM intensity signal variation for all films. Although absolute rms values may increase with film thickness, the variation in topography compared to the overall thickness of the film (percent variation) may be small, as shown here for films >100-nm thick. The percent variation in the NSOM signal also decreases with increasing film thickness.

cence intensity in the film. Figure 6 contains NSOM images (Figure 6a) and concurrently obtained topography (Figure 6b) images of a 100-nm-thick Alq_3 film annealed at 200 °C. As shown in Figure 6c, spectra were taken at the points indicated on the NSOM image in Figure 6a. There are significant intensity variations in the NSOM fluorescence image and intensity variations in the spatially resolved spectra obtained but minimal variation in the position of the fluorescence intensity maxima, which is apparent using the vertical line drawn through the spectra as a reference. Although the topography image of the annealed film is not homogeneous, the marked variations in fluorescence intensity observed are surprising because the topography in the fluorescent and less fluorescent regions appears identical.

RMS Roughness and Absorption vs Film Thickness and Annealing Temperature. The peak fluorescence intensity in our confocal and NSOM images decreases with increasing annealing temperature, particularly with $T > T_g$. This decrease in fluorescence intensity with annealing temperature occurs in all our films, from 10- to 500-nm thick. This is not unexpected. Photodegradation of Alq_3,[16] humidity-induced crystallization,[26] and device operation[3,27] all lead to decreases in initial Alq_3 film fluorescence. This decrease can be attenuated by decreasing the concentration of cationic Alq_3 in the film[3] and encapsulating the Alq_3-based device (isolating it from O_2 and/or H_2O in the air),[28,29] but these methods do not entirely eliminate the decrease in fluorescence efficiency; they merely slow it down. What is interesting in our case is the degree to which the fluorescence and topography vary given the exposure of the entire film to the same annealing temperature.

In the thinner films, darker regions in the fluorescence intensity images occupy larger areas than those found in the thicker films, given the same amount of annealing time. Both the NSOM and confocal images exhibit this trend, but NSOM allows us to examine fluorescence intensity changes by comparing fluorescence images and localized emission spectra with shear force topography images. We observe more pronounced topography changes after annealing the thinner films. There is evidence of crystal formation, with the formation of regularly shaped features, but these changes are less pronounced for thicker films.

Overall trends in the rms roughness value for fluorescence contrast and topography variation are shown in Figure 6. The absolute rms variation for shear force topography increases with thickness for both thin and thick films annealed above T_g, increases for thin films annealed below T_g, and is fairly constant for thicker films annealed below, as shown in Figure 6a. The topography for films annealed at less than T_g remains fairly even throughout (with more variation for thinner films), as shown in Figure 6a. In comparison, for films annealed at 200 °C, the rms value for the topography variation increases with thickness. For films annealed above T_g, the rms value increases more rapidly with thickness for films <100-nm thick. As we observed with the absorption spectra for annealed Alq_3 films, the thinner films (<100-nm thick) are more likely to undergo temperature-induced changes when compared to the thicker, more thermally stable films. The absolute rms roughness value for fluorescence contrast increases approximately linearly for both films annealed at 100 and 200 °C (not shown).

Another way to analyze the rms surface roughness is to compare the variation to the overall thickness of the film, so we used the absolute rms roughness value to

(27) Nguyen, T. P.; Jolinat, P.; Destruel, P.; Clergereaux, R.; Farenc, J. *Thin Solid Films* **1998**, *325*, 175−180.
(28) Popovic, Z. D.; Aziz, H.; Hu, N.-X.; Hor, A.-M.; Xu, G. *Synth. Met.* **2000**, *111−112*, 229−232.
(29) Laubender, J.; Chkoda, L.; Sokolowski, M.; Umbach, E. *Synth. Met.* **2000**, *111−112*, 373−376.

calculate the variation in the fluorescence and topography as a percentage of the overall film thickness (% rms roughness or % variation). Although the absolute rms roughness value does increase with thickness in some cases (shown in Figure 7a), there is clearly less variation in the percent rms roughness value for films greater than 100-nm thick in both films annealed at less than T_g (Figure 7b) and films annealed at greater than T_g (Figure 7c). This is more evidence that thicker Alq_3 films are more thermally stable. When we plot percent rms variation in topography and fluorescence contrast as a function of thickness, we find that thinner films exhibit greater percentage fluctuations in rms values, with a maximum at ≈50 nm and then a slow decrease to fairly constant values for films >250-nm thick.

In conclusion, with the optical spatial resolution made possible by NSOM, we have observed nanoscale effects of annealing temperature on film morphology and fluorescence emission characteristics in thin films (10−500 nm) of the molecular semiconductor Alq_3. Topographic homogeneity, fluorescence homogeneity, and fluorescence intensity changes as a function of annealing temperature and film thickness. Comparing shear force topography and fluorescence NSOM images to each other, we have determined the degree of correlation between topographical and fluorescent features as a function of annealing temperature and initial film thickness. Although annealing temperature is the determining factor in many of these changes, the degree to which the films are altered is affected by the initial film thickness. Films annealed at 100 °C for 1 h were very similar to unannealed Alq_3 films, except for very thin Alq_3 samples (<50-nm thick). In contrast, films annealed at 200 °C ($T > T_g$) exhibited large variations in topography and fluorescence homogeneity. In particular, in thicker Alq_3 films (≈500 nm), we observed the formation of microcrystalline features on the order of 100 nm.

Acknowledgment. This work was financially supported by the David and Lucile Packard Foundation (Packard Fellowship), NSF (CHE-9501773), and by a UCSB Brython Davis Endowment Fellowship to G.M.C.

CM000672O